

4886 288

NEW YORK UNIV NY NEUROMAGNETISM LAB
MAGNETIC FIELDS OF THE CEREBRAL CORTEX, (U)
JUN 80 S J WILLIAMSON, L KAUFMAN

F/6 6/16

UNCLASSIFIED

6

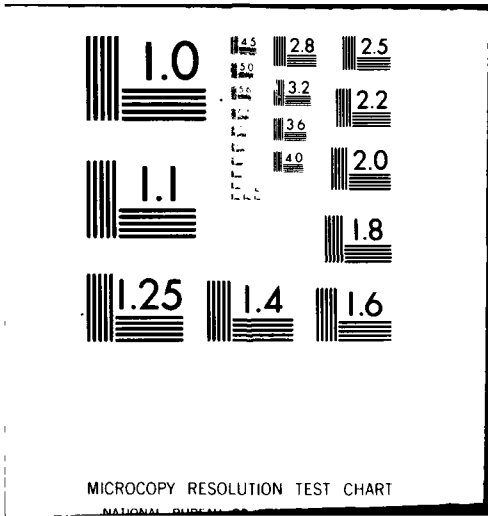
N00014-76-C-0568

NL

1 of 1
Serial



END
DATE
FILMED
8-80
DTIC



MICROCOPY RESOLUTION TEST CHART

NATIONAL BUREAU OF STANDARDS

ADA 086288

DDC FILE COPY.

LEVEL II

12

SECURITY CLASSIFICATION OF THIS PAGE (When Data Entered)

REPORT DOCUMENTATION PAGE

READ INSTRUCTIONS BEFORE COMPLETING FORM

1. REPORT NUMBER 146	2. GOVT ACCESSION NO. AD-A086288	3. RECIPIENT'S CATALOG NUMBER
4. TITLE (and Subtitle) Magnetic Fields of the Cerebral Cortex		5. TYPE OF REPORT & PERIOD COVERED Publication
6. AUTHOR(s) Samuel J. Williamson & Lloyd Kaufman		7. CONTRACT OR GRANT NUMBER(s) N00014-76-C-0568
8. PERFORMING ORGANIZATION NAME AND ADDRESS Departments of Physics and Psychology New York University, Washington Square New York, NY 10003		9. PROGRAM ELEMENT, PROJECT, TASK AREA & WORK UNIT NUMBERS NR 201-209
10. CONTROLLING OFFICE NAME AND ADDRESS Office of Naval Research (Code 441) Department of the Navy Arlington, VA 22217		11. REPORT DATE 15 June 1980
12. MONITORING AGENCY NAME & ADDRESS (if different from Controlling Office) 1251		13. NUMBER OF PAGES 50
		14. SECURITY CLASS. (of this report) unclassified
		15a. DECLASSIFICATION/DOWNGRADING SCHEDULE

16. DISTRIBUTION STATEMENT (of this Report)
Distribution unlimited

DISTRIBUTION STATEMENT A

Approved for public release;
Distribution Unlimited

S DTIC ELECTE D

JUL 8 1980

17. DISTRIBUTION STATEMENT (of the abstract entered in Block 20, if different from Report)

A

18. SUPPLEMENTARY NOTES
To appear in: Biomagnetism, S.N. Ern , H.D. Hahlbohm, and H.L bbig, Eds. (Walter de Gruyter, Berlin), to be published.

19. KEY WORDS (Continue on reverse side if necessary and identify by block number)

biomagnetism	vision
neuromagnetism	hearing
evoked potentials	touch
evoked magnetic fields	cortical sources

20. ABSTRACT (Continue on reverse side if necessary and identify by block number)

The observed patterns over the scalp of magnetic fields evoked by visual, somatic, and auditory stimuli are analyzed to deduce the position and depth of the equivalent current dipole generating source. Expressions are developed for both sphere and half space models for the head, and graphs are presented to correct for the use of a pickup coil of finite diameter. For all three responses, the position of the generating source is deduced to lie in the corresponding primary projection area of the cortex.

111824 (over)

MAGNETIC FIELDS OF THE CEREBRAL CORTEX*

Samuel J. Williamson[†] and Lloyd Kaufman
Neuromagnetism Laboratory
Departments of Physics and Psychology
New York University
New York, NY, 10003, U.S.A.

Dist. Status	
Dist. Status	Unmeasured
Justification	
By _____	
Distribution/	
Availability Codes	
Dist.	Availand/or special
A	

Introduction

This paper focuses on several aspects of neuromagnetic studies of human cortical activity that have proven of particular interest within the last three years. Although we shall refer to each of the papers published so far in the area of magnetic studies of brain activity, our treatment is not in the nature of a review. Elsewhere we shall publish a critical review of all the work in neuromagnetism to date, including comparisons with the more conventional studies of electric potential variations on the scalp (1). The reader is also referred to a complete review of the subject of biomagnetism recently prepared by the present authors which includes a systematic and detailed presentation of the basic theory, experimental techniques, and phenomena (2). An earlier review of biomagnetism has been given by Williamson, Kaufman, and Brenner (3), and a more specialized review of magnetic phenomena of the central nervous system has been authored by Reite and Zimmerman (4).

Background

About 110 years ago Paul Broca found a lesion in the frontal cortex of the right hemisphere of a speechless man's brain. This discovery launched a long search to define the

80 7 3 066

20

relationship between various structures of the brain and specific psychological functions. While the findings resulting from this search have shown that various portions of the brain are related to specific mental processes, none of them have indicated how the brain really works. What is it that a particular structure actually does? Recognizing this problem, psychologists turned to indirect methods in order to discover the answer. For example, the Gestalt psychologists promulgated the doctrine of psychophysical isomorphism which holds that there is a one-to-one relationship between occurrences in the brain and events in perception. They believed that it is possible, from knowledge of states of the brain, to predict what the owner of the brain actually perceives. Since it was not then possible to determine states of the brain, the Gestaltists turned the problem around. Their doctrine enabled them to say that one could discover the states of the brain by studying the perfectly correlated states of perceptual experience. Unfortunately, the program of the Gestalt psychologists foundered on the fact that there appears to be no unique way to determine precisely what it is that the brain does from a study of what it is that the owner of the brain experiences. Ongoing brain processes are far more complicated than what an observer is capable of reporting about his experiences.

Even though there is no way to uniquely determine the brain functions that underly perceptual experience from the study of that experience alone, there have been a number of fruitful guesses. This is not too surprising since neural events do underly perceptual phenomena and some of these phenomena, when properly studied, suggest basic functional mechanisms whose existence may be verified by physiological means.

There are a number of famous examples in which physiological mechanisms were predicted by means of psychological methods. For one, the trichromaticity theory proposed by Maxwell and Helmholtz to account for the facts of color mixture led to

the prediction of the existence of three types of cones, each type with its own spectral response properties. The particular absorption spectra were identified in psychophysical experiments and were subsequently verified by direct physiological measurements. Also, the opponent mechanisms that are now known to be present in the visual system were first postulated by Hering to account for certain phenomena in color vision. The response properties of these mechanisms were identified in psychophysical experiments before actual neurons having the same properties were studied by physiological means. Finally, certain visual phenomena suggested the existence of an inhibitory process because the sensation gotten by stimulation of one retinal place is altered when another retinal place is simultaneously stimulated. This led to the discovery of lateral inhibition in the eye of an invertebrate animal.

The psychophysical methods used to measure the sensitivity of the visual system to various kinds of stimuli and how this sensitivity varies with the conditions of the experiment have been very useful in suggesting mechanisms at various stages in the visual system. These stages involve the photoreceptors, the peripheral neurons and the afferent pathways, and even the brain itself.

Another method often used by psychologists in their investigations of sensory systems is the reaction time method which was first developed by Helmholtz. The total reaction time depends upon the time constants of the receptors, the peripheral neural pathways, and the brain, as well as the time for signals to traverse the efferent neural pathways and cause muscles to contract. The peripheral and the central components involved in the overall reaction time task are notoriously variable. Reaction time is influenced by the expectancy of the subject, his state of alertness and, among other things, the method employed in presenting the stimulus (5). Despite these difficulties, modern psychologists have been

successful in drawing inferences from the reaction time method about the organization of sensory systems. These inferences, as with those made on the basis of measures of sensitivity, require verification in the physiological domain. There is a need for converging experiments in which the methods of psychology and of physiology are both used to evaluate theories concerning the functions that underly perception.

In the past few decades the physiologists developed an extraordinarily powerful tool for investigating the properties of the sensory systems of animals. This is the micro-electrode which is so small that it can sense the activity of a single neuron when it is placed alongside it. Studies of cells within the brain of a living animal led to the astounding discovery that some of them respond to specific types of visual stimuli. Some cells respond to lines or bars of particular orientation, others to moving objects and still others to corners. We shall not go into the details of the many discoveries made possible by means of the micro-electrode. It is sufficient to say that these discoveries created considerable ferment among perceptionists because they suggested that many of the cells have the properties of mechanisms that could underly sensory phenomena. We shall consider but one example here.

Cells in the retina of the cat, for example, may be subdivided into at least two types. One type responds to relatively large stimuli that are presented rapidly to the eye. These are referred to as Y-cells or, sometimes, as transient cells. Another type responds to fine details and are most sensitive to fine patterns when they are moved slowly or presented steadily. They are the so-called X-cells (sustained cells) and are believed to be involved in pattern vision. These results in animals are analogous to psychophysical findings in humans (6). It is clear that some means is needed for physiological verification of the presence of sustained and transient channels in the human visual system.

One physiological measure that can be used with humans is that of detecting potential differences between electrodes attached to the scalp.

Early in this century physiologically oriented scientists sought a direct measure of human brain activity in the hope that it would reveal the locations and mechanisms that underly mental phenomena. The discovery in the 1920s that potential differences between electrodes attached to the scalp fluctuate over time led to the clinically useful characterization of types of potential changes. This discovery of the electroencephalogram was followed by the finding that stimulation of the eyes, the ears and the skin can lead to detectable electrical responses of the brain. In more recent years these evoked potentials in the case of visual stimuli were found to be differentially affected by patterns as opposed to mere changes in the level of illumination of the eye (7). Also, the amplitudes of components of the evoked potential are differentially affected by the state of arousal of the subject. Despite these discoveries, it is still difficult to identify the sources of many components of the evoked responses which may well originate in different parts of the brain. It is clearly necessary to discover whether the components of the complex waveform composing the evoked potential originate in different structures and to what degree they are independent of each other.

The evoked potential is a very coarse measure. Distant populations of cells in the cortex as well as subcortical nuclei of the brain affect electrodes at the scalp because of currents that spread throughout the medium of the brain. These so-called volume currents are so widespread that the signals of widely separated populations become intermixed and their individual behavior cannot be separated or resolved. This limitation is unfortunate, because even though it is possible to perform many ingenious experiments, the interpretation

of their results in terms of findings with microelectrodes is highly speculative. A given effect might be due to the average activity of diverse populations of cells with very different functions. This may be why studies of the evoked voltages between a pair of electrodes generally have not been able to localize the position of the source. One exception is the signal corresponding to the first activity in the cortex, several tens of milliseconds following stimulation. Later we shall cite recent studies using multi-electrode arrays which appear to offer better resolution of later activity in the cortex. Nevertheless, the few instances where it has been possible to establish the location of a source have revealed virtually nothing about the functional aspects of cortical activity, viz. how sensory information is processed. As we shall see, the evoked magnetic response may help ameliorate this problem.

Our understanding of higher levels of brain processes is even more primitive. From a clinical standpoint the electroencephalogram (EEG) which characterizes ongoing electrical activity has proved valuable in diagnosing certain disorders. But very little is known about the sources of these signals or the role of the underlying neural processes. It is not even known whether the EEG contains substantive information related to thought processes or memory. Despite considerable effort in this kind of study, its contributions toward revealing functional aspects of the brain are meager.

The earliest measurements of the magnetic fields associated with brain activity were dedicated to studies of this spontaneous activity, as expressed by the magnetoencephalogram (MEG). This includes work by Cohen (8,9), Reite et al. (10), and Hughes et al. (11, 12). There are some correlations between the temporal and spatial characteristics of the MEG and EEG, especially with regard to the alpha rhythm. But other features display very weak correlations at best. As our purpose in this paper is to consider aspects of cortical

activity, we will not discuss these features of the spontaneous MEG that, though interesting, are not clearly of cortical origin. The reader is referred to the original reports and to three review papers which highlight the similarities and differences (1,2,4) between MEG and EEG measures of spontaneous activity.

Aspects of Instrumentation

As will later become clear there is considerable interest in mapping the pattern of magnetic field in some detail near the scalp. To achieve this, either the subject must move about from one position to another or the magnetic sensor must be moved. For neuromagnetic studies, acceptable field sensitivity at low frequencies can be obtained only by use of a sensor based on the superconducting quantum interference device (SQUID). The SQUID and the superconducting detection coil which directly senses the field of interest are kept at low temperature by immersion in a bath of liquid helium contained within a cryogenic dewar. A contemporary dewar is a rather bulky object because to conserve liquid helium it is designed to provide good thermal insulation and, to minimize the frequency of refilling, it has a modest storage capacity of perhaps 5 liters for several days supply. Nevertheless there are cases where it is not feasible to disturb the subject, and the dewar must be moved. Mapping a field pattern over the scalp becomes a tedious process unless the dewar's suspension is sufficiently flexible. Using three SQUID systems and an orthogonal set of magnetometer coils in the tail of the dewar to detect the three components of the neuromagnetic field would minimize the need to physically reorient the dewar when measuring the field in various directions. But more complicated coil geometries, such as the second-order gradiometer which has

proven useful for measurements in an unshielded environment, have yet to be adapted to multiple axis configurations. Therefore the dewar must be both displaced and oriented to affect measurements about the head.

The well known method of mounting the dewar in a two-axis gimballed support is useful but suffers from an inherent disadvantage whereby the detection coil in the tail of the dewar is displaced horizontally when the orientation is adjusted. A simple design that avoids the worst aspect of displacement is portrayed in the photograph in Fig. 1. The details are sketched in Fig. 2. The dewar is held in a fiberglass cradle which is suspended from an aluminum carriage free to travel horizontally on two sets of orthogonally oriented tracks. The tracks are ground stainless steel rods, and the carriage is supported on them by linear motion Thompson roller bearings. A horizontal run of ~ 70 cm in each direction is possible; and when the desired position is reached the carriage is locked with spring-loaded bicycle brakes (not shown). To minimize any transmission of building vibrations to the dewar, the suspension supported by the carriage is fabricated from fiberglass or wood wherever possible. Vertical movement of the dewar is permitted by a 6 cm diameter cylindrical axle of hardwood that runs between sets of aluminum rollers having double conical shape. The axle is supported by four strands of nylon parachute cord, each rated for 230 kg, that run over a pulley to a lead counterweight. The axle has the additional advantage of allowing rotations about the vertical axis for adjusting the dewar's azimuthal orientation. Friction in the system holds the vertical and azimuthal positions.

For adjustment of the dewar's declination by as much as 45° from the vertical, a system of gears rotates a fiberglass frame with respect to a horizontal yoke fixed to the vertical axle. At the same time the dewar is rotated with respect to the frame in the opposite direction. The frame is



Figure 1. Installation at New York University for measuring evoked magnetic fields of the human brain. The SQUID detection system is mounted within the dewar, suspended over the subject's head. The detection coil is located within the narrow tail of the dewar, which in this illustration is positioned to detect the auditory evoked field.

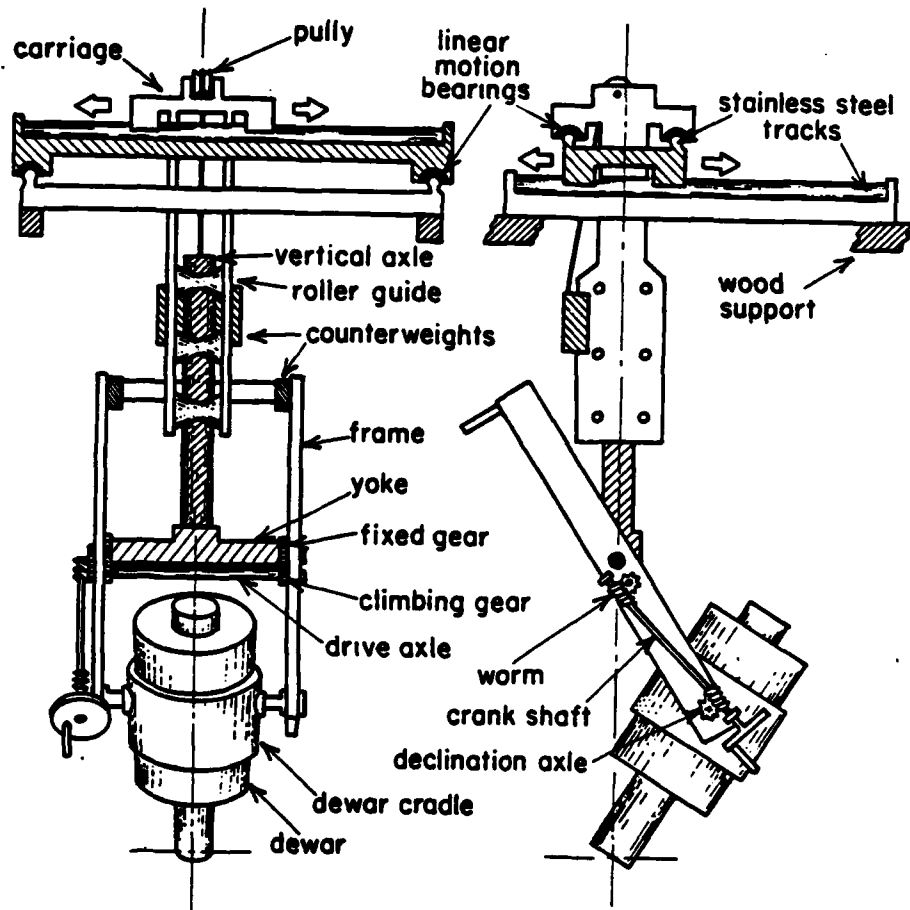


Figure 2. A suspension system permitting translation of a dewar in any of three orthogonal directions and adjustment of the dewar's declination and azimuth without horizontal displacement of the bottom of the dewar. The drawing is not to scale.

counterweighted to minimize the torque required for driving the gears. To effect this rotation a crank and shaft rotate worms which mesh with worm gears on two separate horizontal shafts. One shaft (the declination axle) near the end of the frame rotates the dewar. The other near the center of the frame rotates a pair of climbing gears that mesh with gears fixed to the ends of the yoke. As they rotate they "climb" up or down the fixed gears and thereby rotate the frame. If the dewar is mounted in the carriage so that the distance between the bottom of its tail and the declination axle matches the distance between that axle and the center of the fixed gears, the bottom of the tail remains precisely under the vertical axle. Thus any adjustments of declination or azimuth leave the bottom of the tail at the same horizontal position, as desired. One disadvantage of this simple arrangement is the fact that as the dewar's declination is adjusted the height of the dewar also changes, thereby requiring a compensating adjustment of the position of the vertical axle. In practice this is a small price to pay for the convenience in maintaining the horizontal position during angular adjustments.

The total length of the suspension is about 2.5 m, and when it is fully lowered the dewar is at a convenient height for transferring liquid helium. At the top, wood beams attached to the ceiling support the aluminum frame on which the carriage tracks are mounted. This suspension has been in use for one year, and only once were vibrations seen to contribute to the noise. A resonance of the suspension at about 12 Hz appeared for a particular dewar position, but this cannot be reproduced reliably. The heavy damping provided by lossy mechanical elements appears to be a virtue as compared with, say, an all aluminum construction. Some "non-magnetic" stainless steel components such as gears and shafts are located only ~ 30 cm from the detection coil (a second-order gradiometer), but any magnetic noise contributed by these paramagnetic objects is less than ~ 20 fT/Hz^{1/2} in the

frequency domain above 10 Hz, which is negligible for this system.

Part of the motivation for constructing a dewar suspension of this type is to obtain data from which field maps can be made in order to determine where the current source for a neuromagnetic field lies. In cases to be documented later, the field is often observed to have a maximum outward strength at one position on the scalp and a maximum inward strength at another position close by. This suggests the source might be modeled by a localized current element lying midway between the two extrema. One might expect to deduce the depth of this current element from the dimensions of the pattern, and determine its strength from the intensity of the field at one of the extrema. The next two sections explore some of the relevant features of the field patterns for the most elementary form of a current element: the current dipole.

Current Dipole in a Half Space

The law of Biot and Savart specifies how the current density within each infinitesimal volume in space contributes to the magnetic field at a point (13). In a non-magnetic medium the magnetic induction is given by:

$$d\vec{B} = \frac{\mu_0}{4\pi r^3} \vec{J} \times \vec{r} d^3r, \quad (1)$$

where \vec{r} is the position vector from the current density \vec{J} to the point of interest. If we imagine at a given instant that \vec{J} is non-zero within only a small region of space relatively far from the point of interest, \vec{r} can be taken as a constant, and the integral over space that gives the total field \vec{B} involves just the volume integral of \vec{J} . This integral completely characterizes the source so far as the information available in the magnetic field is concerned. The integral

has the dimensions of current-length and the unit of the ampere-meter. It is called a current dipole by analogy with the term charge dipole of electrostatics, which has the dimensions of charge-length. We let \vec{Q} stand for the current dipole vector. Its direction coincides with the flow of current represented by \vec{J} . The current dipole is a simplified model source describing the movement of charge over a short distance. Eq. 1 predicts that the field describes circles about \vec{Q} in planes normal to \vec{Q} . The field strength at a point lying a distance r from \vec{Q} in a direction making an angle ψ with respect to \vec{Q} is

$$B = \frac{\mu_0 Q \sin \psi}{4\pi r^2} \quad (2)$$

The magnetic field thus decreases as the inverse square of the distance. By contrast the field from a magnetic dipole falls off more rapidly, as the inverse cube of the distance.

The movement of charge associated with the conversion of energy from a non-electrical form to an electrical form is called an impressed current. For example, the diffusion of sodium ions through channels in a nerve membrane is a result of an existing transmembrane difference in ion concentrations established by metabolic processes. As a consequence of the diffusion there is a buildup of electrical potential energy owing to the accumulating charge imbalance. Thus chemical energy, represented by the initial difference in chemical potential for the ions, is converted into electrical potential energy. Such ion movement constitutes an impressed current. The current dipole can represent a localized impressed current, and thereby describe a biological source of magnetic field.

A current dipole in human tissue sets up potential gradients in the surrounding conducting medium. By Ohm's law a current will flow as a passive response to this gradient. This so-called volume current flows in the opposite sense to the current dipole, moving from the head of the vector to its

tail, and has the effect of insuring that there is no buildup of charge at the head or tail. Fig. 3 illustrates the situation in an infinite homogeneous medium. Cohen and Hosaka pointed out that the volume current represents the sum of a radially diverging current at the head and a radially converging current at the tail, and each by Eq. 1 produces no magnetic field (14). Consequently everywhere in a homogeneous medium without boundaries the magnetic field is due to the current dipole alone and is specified by Eq. 2.

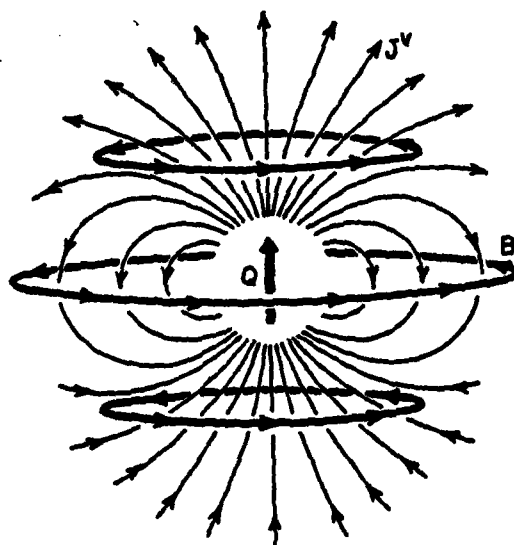


Figure 3. Current dipole \vec{Q} in a homogeneous conducting medium with its magnetic field \vec{B} and associated volume current density \vec{J}^v .

7

However in the more general case of an inhomogeneous medium, the perturbation of the volume current can give rise to a magnetic field. This has been shown explicitly by Grynspan and Geselowitz (15) for any space divided into domains of differing but homogeneous electrical conductivity. Moreover in certain symmetrical situations the volume current can produce an equal but opposite field to that of the current dipole. Then the net external field is zero. Baule and McFee (16) showed that this occurs in situations of axial symmetry. One example is a dipole in a conducting half space (where the region $z < 0$ has finite conductivity but the region $z > 0$ is a vacuum), provided that the dipole is oriented perpendicular to the surface. Another example is a dipole in a slab of infinite extent, oriented perpendicular to the two faces of the slab. In these cases an external field is produced only if the dipole has a component tangential to the surface. The example of the half space is of particular interest, because it may approximate the situation in the brain when an impressed current lies close to the skull. If a dipole lies a distance d beneath the surface of a half space and is oriented in the $+y$ direction, the normal component of the field at the surface is (16):

$$B_z = \frac{\mu_0 Q}{4\pi d^2} \cdot \frac{x}{(1+x^2+y^2)^{3/2}}, \quad (3)$$

where x and y are coordinates on the surface expressed in the units of d so that they are dimensionless. By considering symmetry properties of the volume currents, Cohen and Hosaka (14) have shown that B_z anywhere outside the conducting half space is given by Eq. 3, provided that d is then replaced by the distance $z+d$, where z is the distance of the point of interest from the surface of the half space. By extension of these arguments, Eq. 3 remains valid if there are intervening slabs of infinite extent and differing conductivity (representing the skull and scalp) between the half space and the point of interest where the field is measured. These

media between the current dipole and a field sensor cause no distortion of the normal component of the magnetic field.

The field pattern described by Eq. 3 is illustrated in Fig. 4 by contours of constant field (isochamps). The positions of maximum field intensity lie on the x-axis at $x = \pm 2^{-\frac{1}{2}}$. The total distance Δ between these extrema is related solely to the value of d , since

$$\Delta = 2^{\frac{1}{2}}d. \quad (4)$$

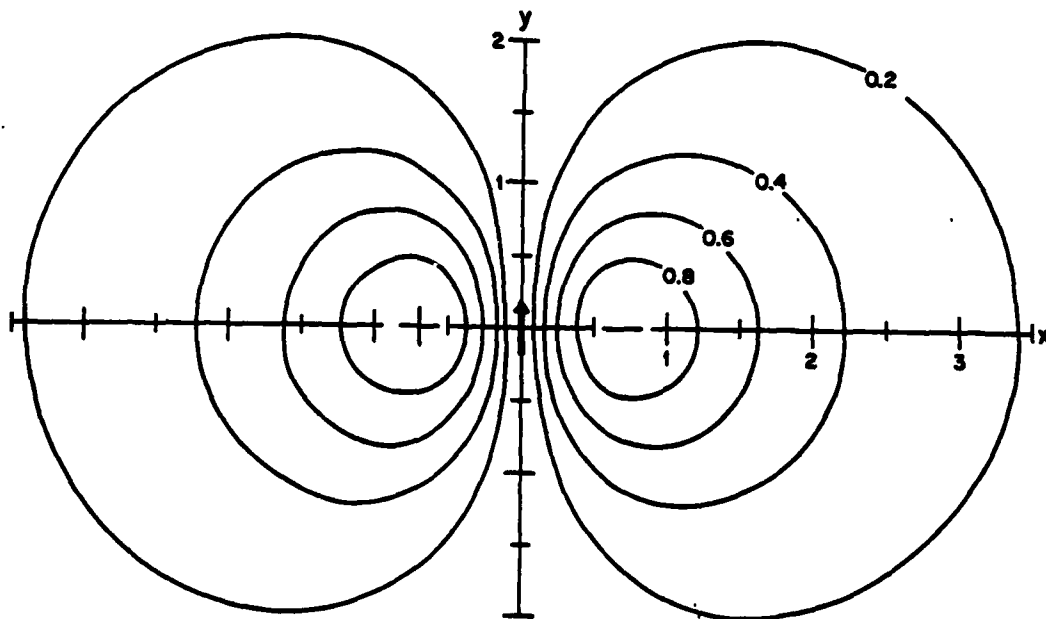


Figure 4. Isochamps for the field B_z when a current dipole lies at a depth d below the z -plane of measurement in a homogeneous conducting half space and is oriented in the $+y$ direction. Both x and y are expressed in the units of d .

The field at each extremum has the magnitude

$$B_m = 0.385 \frac{\mu_0 Q}{4\pi d^2} \quad (5)$$

Thus with a knowledge of 'd, obtained from a measurement of Δ , together with a measurement of the maximum field B_m the magnitude of Q can be deduced.

Although only the tangential component of \vec{Q} contributes to the external magnetic field, both tangential and normal components contribute to the electric potential at the surface of the half space. This potential is an expression of the volume current that spreads from the current dipole. The source of the volume current can be imagined equivalently as being a charge dipole of moment $\vec{p} = \kappa \epsilon_0 \vec{Q} / \sigma$ whose charge separation equals the length of the current dipole. Here κ is the dielectric constant of the medium, σ is the conductivity of the medium, and ϵ_0 is the permittivity of free space. The volume currents flowing outward from the positive charge and inward toward the negative charge match the impressed current of the dipole itself. The resulting potential V at the surface can be deduced by conventional arguments based on assuming an image dipole to satisfy the boundary condition of no outward flow. If \vec{Q} is inclined from the z-axis by an angle θ' toward the +y-axis we can express the contribution of the tangential component of the dipole as

$$V_T = \frac{Q \sin \theta'}{2\pi \sigma d^2} \left| \frac{y}{(1 + x^2 + y^2)^{3/2}} \right. \quad (6)$$

This has precisely the same form as Eq. 3 for B_z but the pattern is rotated by 90° about the z-axis. Moreover there will be a contribution to the potential from the component of the dipole that is normal to the surface:

$$V_N = \frac{Q \cos \theta'}{2\pi \sigma d^2} \left| \frac{1}{(1 + x^2 + y^2)^{3/2}} \right. \quad (7)$$

The isopotentials shown in Fig. 5 vary in a complicated way as the angle of inclination θ' is varied. One remarkable feature is the dominant influence exerted by the end of the dipole which is closest to the surface. Moving from the symmetrical tangential orientation of $\theta' = 90^\circ$ by reducing θ' by only 15° produces a factor of 2 difference between the magnitudes of the potentials at the two extrema. A reduction to $\theta' = 60^\circ$ leaves only a hint of the weaker region. Only a very careful and sensitive mapping of the isopotentials could reveal the presence of a tangential component for orientations $\theta' < 60^\circ$. In principle surface potential measurements could reveal both normal and tangential components; however in practice the normal component is emphasized, unless the dipole is oriented to within a few tens of degrees of the tangential direction. In this sense the magnetic measurements are complementary, since they detect only the tangential component.

Averaging by the Pickup Coil

A SQUID system provides an output signal that is proportional to the total magnetic flux which threads its detection coil. For a magnetometer or a gradiometer having a sufficiently long baseline this is the flux which passes through the pickup coil. That is, the output is a measure of the average field \bar{B} within the coil. In studies of the field pattern from a current dipole it is important to know how faithfully $\bar{B}(\vec{r})$ describes the actual spatial variation of the field $B(\vec{r})$. One expects important distortions to appear if the diameter "2a" of the pickup coil is so large that it is comparable to the distance Δ separating the two field maxima on the surface of the skin. In the case where the situation can be approximated by the conducting half space, which we consider in this section, the measured value \bar{d} given by the observed variation of \bar{B} would predict by Eq. 4 a much greater value \bar{d} of the dipole's depth than the actual depth d . And

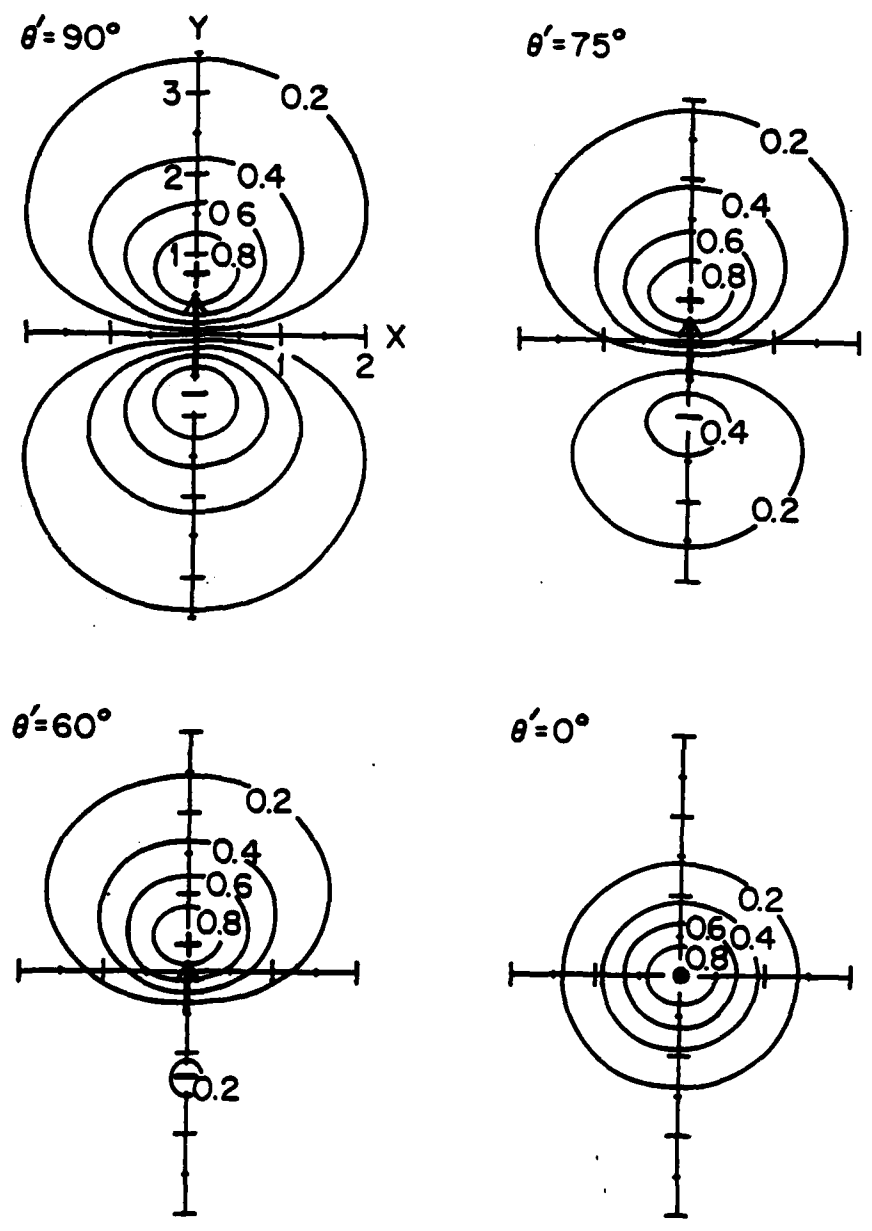


Figure 5. Isopotentials on the surface of a homogeneous conducting half space arising from the volume currents associated with a current dipole at a depth d and inclined from the $+z$ -direction by an angle θ' toward the $+y$ -direction.

even if one knew this correct depth, using the measured value of the field extremum \bar{E}_m in Eq. 5 would lead to an incorrect value \bar{Q} for the dipole strength.

To evaluate how to correct for using a pickup coil of finite size we have found it convenient to apply lead field theory as developed by Baule and McFee (16,17) and Plonsey (18). In this approach one assumes that there are two impressed sources: a current $I_R \exp(j\omega t)$ that is passed through the pickup coil and a second current $\vec{J}^i(\vec{r}) \exp(j\omega t)$ that is the impressed current density, both varying sinusoidally at a low frequency ω . From considerations of the field equations describing the distribution of electric and magnetic fields Plonsey has obtained an expression that predicts the voltage that would be induced in the pickup coil if $\vec{J}^i(\vec{r})$ were the only source present. This expression contains information about the shape of the pickup coil in that it includes the electric voltage $\vec{E}_L(\vec{r})$ that would be induced at each point in space by the imagined flow of I_R . $\vec{E}_L(\vec{r})$ is called the lead electric field. We generalize Plonsey's Eq. 20 to obtain an expression for the flux produced in the pickup coil, which is of more direct interest for SQUID systems than the form of his equation:

$$\phi = - \frac{1}{I_R} \int \frac{\vec{E}_L(\vec{r}')}{j\omega} \cdot \vec{J}^i(\vec{r}') d^3r'. \quad (8)$$

Often Eq. 8 is written in terms of the ohmic current distribution that would be produced by the lead field: $\vec{J}_L(\vec{r}) = \sigma \vec{E}_L(\vec{r})$. Here \vec{J}_L is known as the lead current. The lead electric field is advanced in phase by $\pi/2$ with respect to I_R , since the field is caused by Faraday induction. Thus the expression $\vec{E}_L/j\omega$ has the same phase as I_R , and we can no longer be concerned with the phaser notation. If a positive value is obtained when evaluating the right hand side of Eq. 8 for a given distribution of primary current, the net flux produced in the pickup coil by this current has the same

sign as the flux produced within the coil by the imagined I_R . Because E_L is proportional to I_R the actual value chosen for I_R is irrelevant for the calculation, and it could be taken equal to unity.

A straightforward application of Eq. 8 involves many difficulties, not the least of which is the fact that the variation of electrical conductivity within the body must be taken into account. Even for the homogeneous half space of interest to us, a surface integral of the lead magnetic field must first be solved in order to deduce E_L . Unfortunately, expressions for the magnetic field pattern from even a circular pickup coil are complicated. It is much more convenient to recast Eq. 8 into a form that depends on the lead vector potential $\vec{A}_L(\vec{r})$ produced by the flow of I_R through the pickup coil: This potential is related to the lead magnetic induction by $\vec{B}_L = \nabla \times \vec{A}_L$ and to the lead electric field by $\vec{E}_L = -\partial\vec{A}_L/\partial t = -j\omega\vec{A}_L$. If the coil is oriented with its axis perpendicular to the surface of the half space, no complications arise from the effects of the surface. Then Eq. 8 can be rewritten as

$$\phi = \frac{1}{I_R} \int \vec{A}_L(\vec{r}') \cdot \vec{J}^i(\vec{r}') d^3r'. \quad (9)$$

This relationship is implicitly contained in lead field calculations reported by Malmivuo (19) for several configurations of detection coils. This equation indicates that the orientation for which a primary current density \vec{J}^i produces the greatest flux ϕ is along the direction of \vec{A}_L at its position. If \vec{J}^i is parallel to \vec{A}_L , the flux is in the same direction as that produced in the coil by the imagined I_R ; if antiparallel, it is in the opposite direction.

To arrive at our goal of calculating the effect of a pickup coil of finite size on the observed field pattern from a current dipole, we integrate Eq. 9 when the dipole is located at the position \vec{r} :

$$\phi = I_R^{-1} \vec{A}_L(\vec{r}) \cdot \vec{Q}(\vec{r}). \quad (10)$$

This remarkably simple expression is also particularly useful. A detection coil with axial symmetry produces circular patterns of A_L about that axis. For example a circular loop of radius "a" produces a vector potential directed circularly in the same sense that I_R flows around the coil. Its magnitude is given by (20)

$$A_L(r) = \mu_0 \pi^{-1} a (a^2 + r^2 + 2ar \cdot \sin \alpha)^{\frac{1}{2}} \left[\frac{(2-k^2)K(k^2) - 2E(k^2)}{k^2} \right], \quad (11)$$

$$\text{where } k^2 = 4ar \cdot \sin \alpha (a^2 + r^2 + 2ar \cdot \sin \alpha)^{-1},$$

$$r = d(1+x^2+y^2)^{\frac{1}{2}},$$

$$\sin \alpha = (x^2+y^2)^{\frac{1}{2}} d/r.$$

In these expressions "r" is the distance of the point of interest from the center of the coil, and α is the angle between \vec{r} and the coil's axis. $K(k^2)$ and $E(k^2)$ are the complete elliptic integrals of the first and second kind, such that in the limit of small "a" (or small k^2) the expression in square brackets reduces to $\pi k^2/16$.

We now apply the expression in Eq. 10 to the case where the coil is placed at the surface of the half space, and its center lies at the position (x,y) in the z=0 plane. A current dipole Q lies on the z-axis at z = -d and is oriented in the +y direction. We choose to express our results in terms of the averaged detected field as defined by

$$\bar{B}_z = \phi/\pi a^2. \quad (12)$$

Then Eq. 11 yields:

$$\bar{B}_z = \frac{\mu_0 Q}{4\pi d^2} \cdot \frac{x}{(x^2+y^2)^{\frac{3}{2}}} \cdot \frac{4d^2}{\pi a} (a^2+r^2+2ar \sin \alpha)^{-\frac{1}{2}} \cdot \left[\frac{(2-k^2)K(k^2) - 2E(k^2)}{k^2} \right] \quad (13)$$

In the limit of small "a" this expression reduces to that in Eq. 3, so that $\bar{B}_z(x,y)$ is an exact representation of $B_z(x,y)$. But Eq. 13 is correct for any value of "a", and therefore it can be used to assess the effect of measuring the field with a large pickup coil. For simplicity we consider the variation of the measured field as the coil is moved along the x-axis ($y=0$), where it will pass through the most intense region of field. Fig. 6 illustrates how for larger coils the maximum observed value \bar{B}_m is reduced and its position $\bar{\Delta}/2$ shifts further away from the dipole's position.

From these results we have deduced correction factors that can be used to adjust experimental results to compensate for use of a pickup coil of finite size. Fig. 7 provides a correction factor d/\bar{d} that can be applied to calculate the actual depth "d", given the empirical value $\bar{d} = \bar{\Delta}/2^{\frac{1}{2}}$ from Eq. 4. The figure also gives the correction factor Q/\bar{Q} for obtaining the actual strength of the dipole given the empirical value $\bar{Q} = 4\pi d^2 \bar{B}_m / 0.385\mu_0$ from Eq. 5. Note that in the expression for \bar{Q} the actual value of the dipole's depth appears and not the empirical one. The corrections for depth and strength are only on the order of 6% when the coil diameter $2a$ is half of the observed separation Δ between field extrema. But the corrections escalate sharply when the diameter approaches the value of Δ .

Current Dipole in a Sphere

When an element of neural current lies an appreciable distance

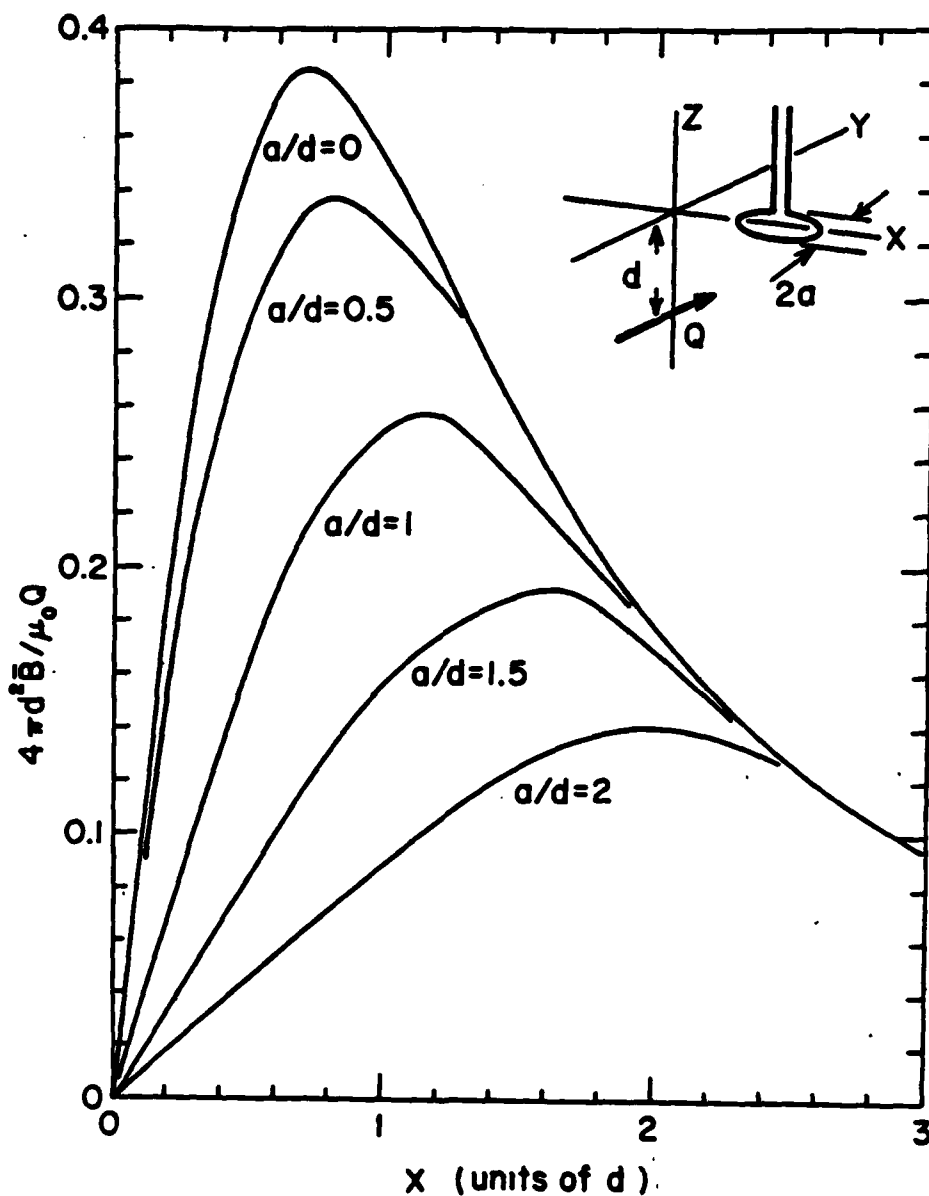


Figure 6. Measured average field \bar{B}_z for positions along the $+x$ -direction when a current dipole lies at a depth d below the z -plane of measurement in a homogeneous conducting half space and is oriented in the $+y$ -direction. The effect of using a pickup coil of finite diameter $2a$ is shown, as predicted by Eq. 13.

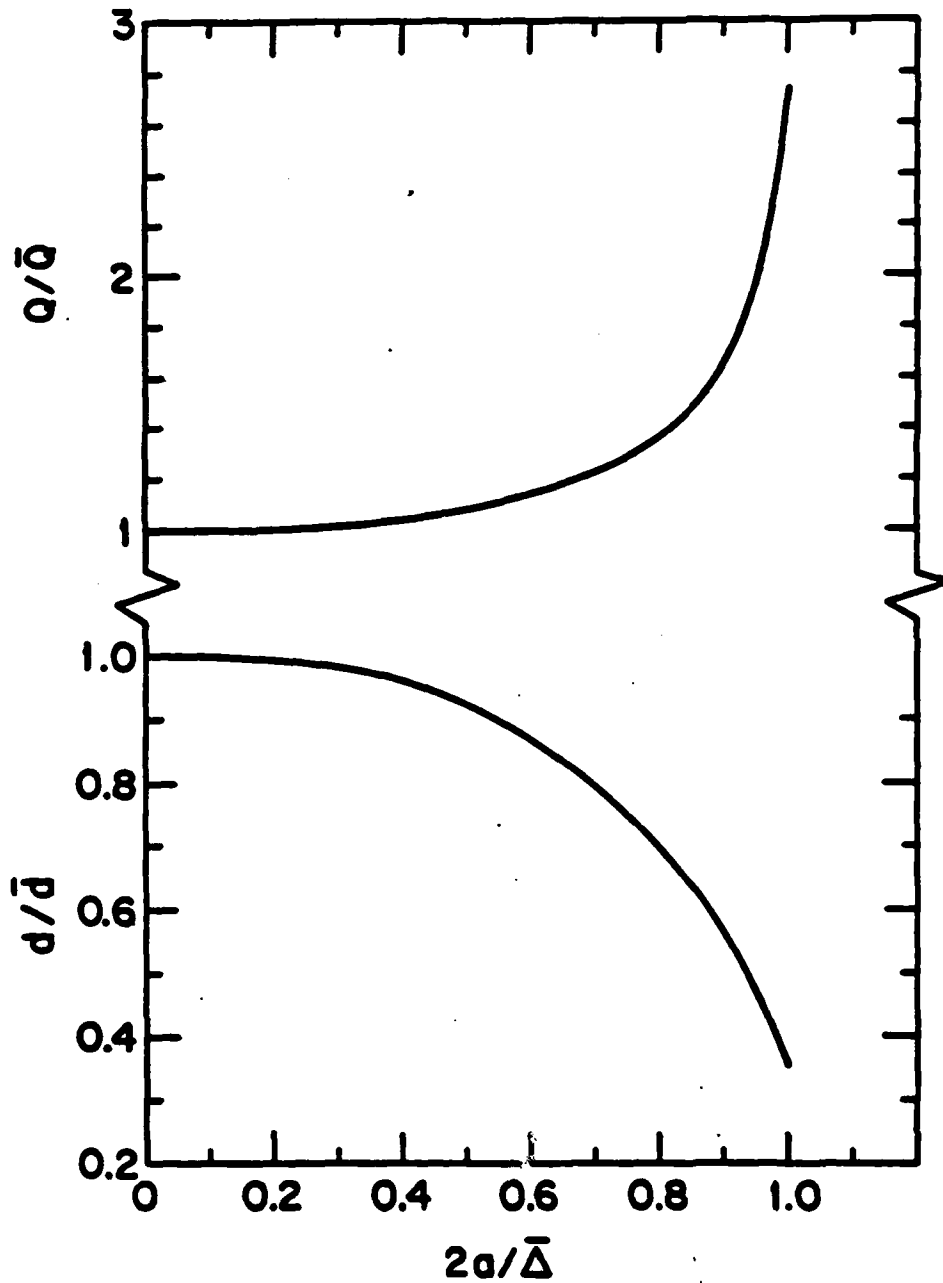


Figure 7. Factors for obtaining the correct depth d and strength Q of a current dipole in a half space from the values of \bar{d} and \bar{Q} deduced from measurements of the average field obtained with a pickup coil of finite size.

beneath the scalp we can expect the model of a current dipole in a half space to be invalid. The curvature of the boundary of the conducting medium becomes an important feature.

Consequently a better model might be a current dipole within a conducting sphere. In this section we consider how features of the observed field pattern can be applied to deduce the depth and strength of a dipole. A comparison of these results with those of the preceding section will show when the influence of the curved boundary becomes important.

The demonstration by Baule and McFee (2) that a current dipole produces no external field in a situation of axial symmetry has important consequences for the sphere model. It predicts for example that a radially oriented dipole cannot be detected magnetically, because the field from its volume current just cancels the field from the dipole itself. Also significant is its prediction that a dipole at the center of the sphere produces no external field. From continuity arguments we expect that the field from a tangentially oriented dipole will diminish toward undetectable levels as the dipole is moved toward the center. Thus the magnetic technique will not directly detect deep-lying sources. Tripp (21) has shown that if the shape of the boundary departs slightly from that of a perfect sphere there is a correspondingly small change in the field pattern. In other words, predictions based on the sphere model are not dramatically affected if there are small departures from the ideal symmetrical boundary.

Grynszpan and Geselowitz (15) have deduced an expression for the magnetic scalar potential outside a sphere when a tangentially oriented current dipole is at a distance "b" from its center. The result is independent of the radius R of the sphere (if $R > b$). Thus R can denote instead the radial distance to the point of interest where the field is measured, with the sphere having a smaller radius. Concentric inhomogeneities either at shorter or longer radii than "b" do not alter the external field pattern (15). Therefore the head can be modeled by concentric spherical shells of differing but homogeneous conductivity to represent such features as the cerebrospinal fluid, skull and scalp at radii exceeding

"b", and the field pattern outside remains undisturbed. The situation will be described by a spherical coordinate system as depicted in the inset of Fig. 8. We let θ denote the angle of declination toward the position of field measurement, and ϕ denote the azimuthal angle with respect to the

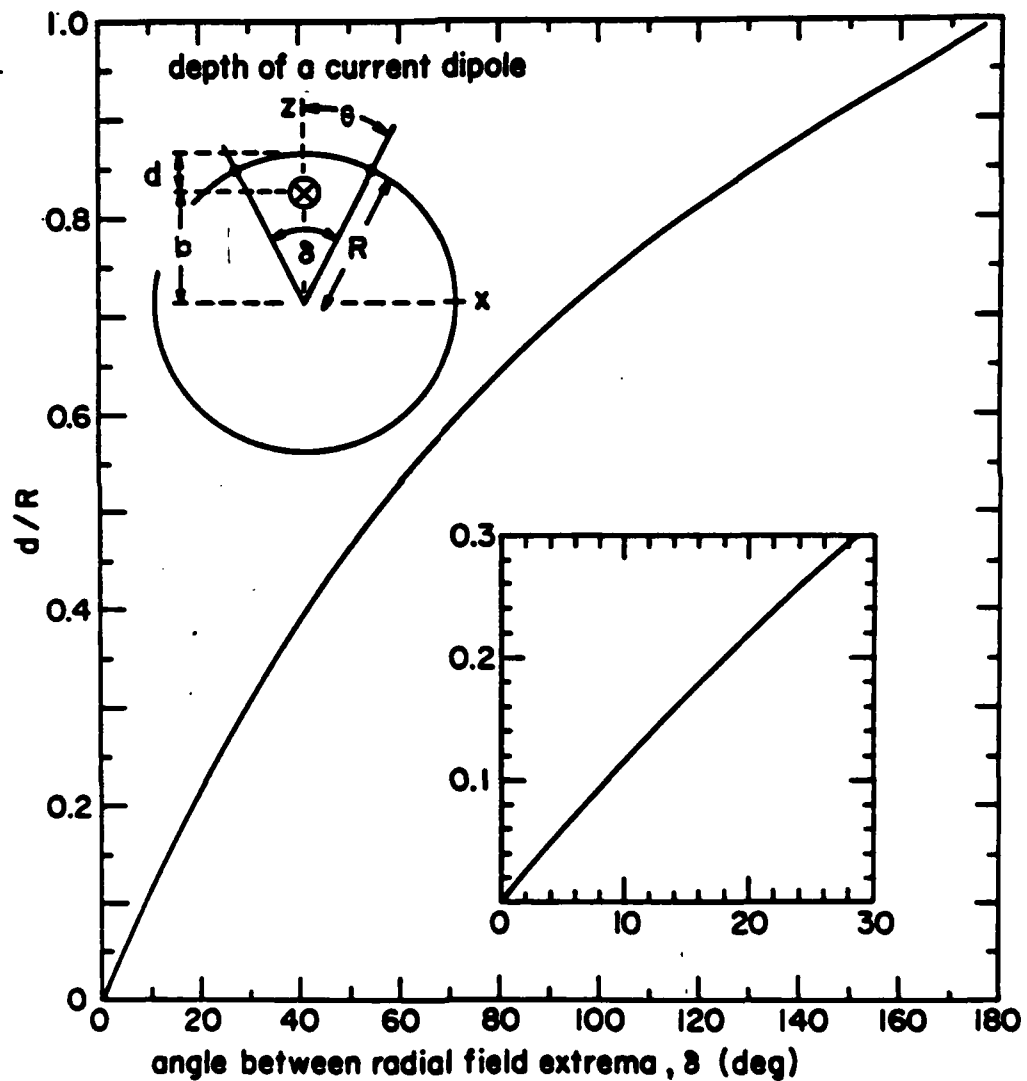


Figure 8. The depth d below the radius of measurement R for the position of a current dipole in a conducting sphere as determined by the angular span δ between the two positions of most intense radial field B_r .

x-axis. The "depth" of the dipole is $d = R - b$. From Eq. 30 of reference 15 we obtain an expression for the radial field:

$$B_r = \frac{\mu_0 Q}{4\pi d^2} \frac{\frac{b}{d} \cos\phi \sin\theta}{\left[1 + \frac{2bR}{d^2} (1 - \cos\theta)\right]^{3/2}} \quad (14)$$

This is equivalent to Eq. 22 of reference 22 which has been derived by another method. The correspondence between this expression and that written in Eq. 3 for the half space model becomes apparent if we rewrite the latter as

$$B_z = \frac{\mu_0 Q}{4\pi d^2} \frac{\frac{R'}{d} \cos\phi \sin\theta}{\left[1 + \left(\frac{R'}{d} \sin\theta\right)^2\right]^{3/2}}, \quad (15)$$

where R' is the radial distance to the point in the z -plane in which the field is measured. In the limit when the dipole is at a shallow depth ($d/R \ll 1$ and $\theta \ll 1$) Eq. 14 becomes identical to Eq. 15. In this limit the predictions of the sphere model reduce to those of the half space model.

When mapping the component of a neuromagnetic field that is normal to the scalp it is easiest to identify the regions where the field is strongest. In the sphere model, Eq. 14 predicts that this occurs at a declination θ_m where the magnitude of B_r is maximum, as given by the solution to

$$\frac{d^2}{2(R-d)R} = \frac{3}{2 \cos\theta_m} - \frac{\cos\theta_m}{2} - 1 \quad (16)$$

What the experimenter can directly measure is the total angular span $\delta = 2\theta_m$ between the positions of maximum inward and maximum outward field. The dipole lies on the radius midway between these two positions. Its depth is given by the curve in Fig. 8 as determined by solutions to Eq. 16 for various values for the total span. Thus from a measurement of δ , the depth of the dipole below the radial distance of the pickup coil can be deduced.

As the depth increases and the dipole approaches the center of

the sphere, the angular span between field extrema tends toward 180° . But as remarked earlier, the strength of the field diminishes toward zero in the limit $d/R \rightarrow 1$, so it will be impossible to detect central sources if the sphere model is applicable. This effect of the spherical boundary in weakening the maximum field through its effect on the volume current is dramatically illustrated in Fig. 9. For the half

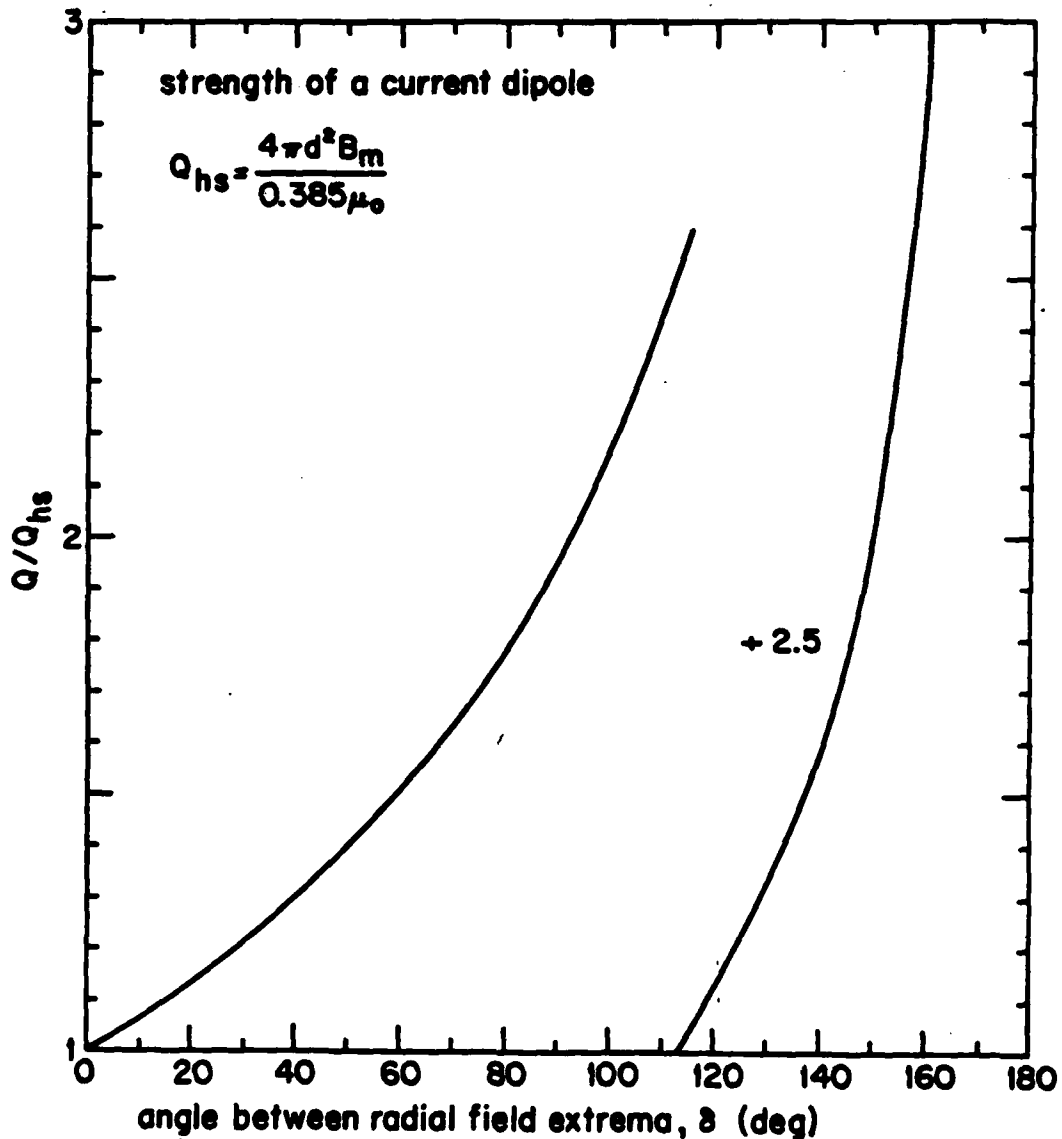


Figure 9. The strength Q of a current dipole in a conducting sphere as determined by the magnitude B_m of the most intense radial field at either extremum at the radius of measurement R , with the depth d of the dipole given by the curve in Fig. 8.

space, the maximum field B_m normal to the surface can be used to predict the strength of the current dipole as given by Eq. 5. Were the same formula to be used for measurements on a sphere with the maximum value of B_r inserted in place of B_m , the deduced value denoted by Q_{hs} underestimates the actual strength of the dipole. Fig. 9 provides the correction factor for how much stronger the actual Q is. For example, when the angular span between extrema is $\delta = 90^\circ$ the dipole has an actual strength that is twice the value of Q_{hs} given by Eq. 5. In making this calculation the value of the maximum radial field and the actual value of "d" given by Fig. 8 should be used. For a span of $\delta = 150^\circ$ the actual strength is 5 times greater than is given by Q_{hs} calculated from Eq. 5.

In this section and the preceding one we have summarized how the position and strength of a current dipole source are determined by the positions of the field extrema and by the strength of the field at either extremum. However the human head is neither a sphere nor a half space, and consequently these results should be applied with caution. For a specific application, an intercomparison of the predictions of the two models will provide some insight as to their sensitivity to differing boundary conditions. But the results do not give any hint of the possible importance of non-concentric internal inhomogeneities within the brain and the angular variation in skull thickness. The field pattern from more complicated model sources involving multiple arrays of current dipoles have been computed by Cuffin and Cohen (23). They have also calculated the lead fields for several types of magnetic detection coils and scalp electrode arrays, based on a multiple concentric shell model for the head (24).

Evoked Fields

Magnetic fields which appear near the scalp in response to a sensory stimulus have attracted considerable interest. Sensory

evoked brain responses, originating at the cortical level, are believed to be among the simplest of neural signals and therefore provide the best opportunity for gaining a foothold on the functional organization of the brain. These signals, however, are extremely weak (~ 100 fT) and in some situations are masked by the ongoing spontaneous activity of the brain. Therefore signal processing techniques have been applied to average the responses to many identical stimuli applied in sequence in order to bring the signal of interest above the noise. An "evoked response" in most cases implies an "averaged evoked response."

Two types of stimuli may be used. The first is an intermittently repeated stimulus where the effect of one stimulus has enough time to disappear before the presentation of the next. The response that is time-locked to each stimulus is called the transient response. It is a complex wave which contains positive and negative peaks, each of which may be characterized by its delay (latency) following the stimulus. The second type of stimulus is periodic and presented at a repetition frequency so high that the effect of one stimulus has not worn off before presentation of the next. This leads to the so-called steady state response (25). It is represented by a response which is periodic at the frequency of the stimulus or its harmonics and is characterized by the amplitudes and phases of its components. Usually only the amplitude and phase of the response at the fundamental frequency has been investigated in detail. The transition between transient and steady state response is believed to occur for stimulus rates of ~ 4 Hz, depending on the type of stimulus. The response of a linear system is completely determined either by its transient response or a knowledge of its steady state response at all stimulus frequencies. Human sensory systems are not linear, and therefore it is not known whether the two types of stimuli provide equivalent information.

It is thought that activity evoked in the cortex of the brain by a sensory stimulus produces the observed scalp potentials and perhaps magnetic fields through the polarization of large numbers of cells. The cortex, which is only 1-3 mm thick, has a cellular organization whereby pyramidal cell bodies are aligned transverse to the cortical layer with their long apical dendrites extending outward toward the surface. A dendrite when depolarized as a consequence of synaptic activity may establish a graded potential until the threshold for the action potential is surpassed. In this condition the altered conductivity of the cell membrane sets up an extracellular current that flows toward the dendrite, which acts as a "sink" for the current. The cell body, a "source," remains electrically positive, and the dendrite relatively negative. The columnar organization within the cortex thus may support a current transverse to the cortical surface in regions where pyramidal cells are excited that produces an external magnetic field. Other neural elements such as stellate cells probably do not contribute to net current densities owing to their random orientations.

If this polarization current is indeed the origin of the evoked magnetic field, the convolutions of the cortex present a complicated geometry which should have an important influence on the observed field patterns. Fig. 10 shows that three of the most accessible sensory areas lie near or within deep fissures of the cortex, where currents lie tangential to the scalp. Thus from considerations mentioned earlier concerning the magnetic field from a current dipole and its volume current in either a half space or sphere we should expect neural activity near these fissures to be emphasized in the patterns of evoked field. Some recent analyses of evoked scalp potentials have taken into account the topology of these fissures when dealing with sources that are believed to lie within their depth (see for example reference 26).

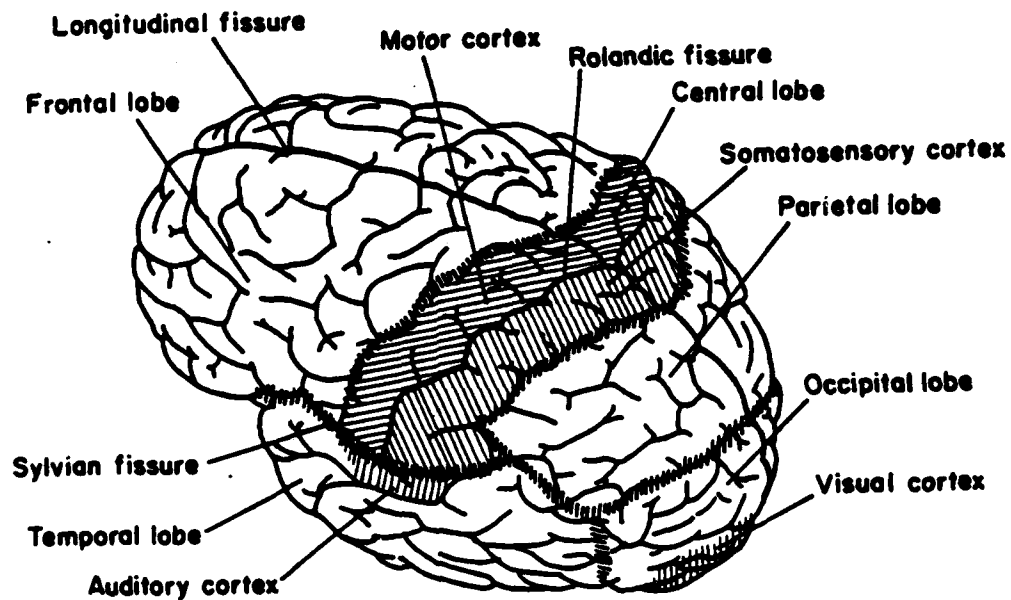


Figure 10. Surface of the brain showing its principal fissures and sensory projection areas of the cortex.

Visually Evoked Field

The first observations of magnetic responses were achieved with visual stimuli. The subject observed either brief flashes of light or a pattern of changing luminance presented on the face of an oscilloscope (27-29). One interesting finding in the steady state visually evoked field (VEF) reported in the initial study of Brenner *et al.* (28) is a sharper localizability over the occipital area near the visual cortex as compared with the visually evoked potential (VEP),

which can be observed as far as frontal areas of the head. Subsequent investigations of transient VEFs by Zimmerman et al. (30) in which magnetic and potential responses were directly compared on the same subjects showed that the VEF extended into posterior parietal and temporal areas but nevertheless was significantly more confined than the VEP.

The temporal features of the VEF have revealed important evidence concerning the functional organization of the visual system in humans. Williamson et al. (31) found that the latency of the steady state response varies with features of the stimulus pattern. The stimulus was a grating pattern formed by a sinusoidal variation of the luminance across the face of an oscilloscope. It was presented in the "contrast reversal" mode whereby the grating is periodically shifted sideways by half a spatial wavelength, thereby causing regions of higher luminance to be replaced by regions of lower luminance. As the overall average luminance remains unchanged, the stimulus is simply one of a changing pattern and is characterized by the spatial frequency of the grating. The latency of the neuromagnetic response was found to increase from ~ 80 ms for a grating of low spatial frequency (about 1 cycle of luminance variation encompassed within 1 degree of visual angle) to more than ~ 120 ms for a high spatial frequency (about 5 cycles/degree). This observation appears significant because a similar variation was reported by Breitmeyer (32) for the reaction times of subjects when suddenly presented by the same types of gratings of various spatial frequencies. The reaction times being consistently 115 ms longer than the neuromagnetic latencies, it is natural to associate the 115 ms with the motor response time that follows activity in the visual cortex. The latency thus represents the sensory response time and appears to be a significant measure of physiological activity.

Visual stimuli are particularly useful for studies of sensory processes because both pattern and presentation rate can be

varied separately. For instance, the dependence of the neuro-magnetic latency on spatial frequency is found to disappear if the stimulus presentation rate is sufficiently rapid (33). This behavior provides the first physiological evidence for tuned transient and sustaining channels in the human visual system as suggested by psychophysical and animal studies. Additional results of this type of study are presented by Brenner et al. in these Proceedings (34).

Here we shall concentrate on the information that can be obtained about the locations of the sources of the evoked field. In carrying out measurements of evoked fields in our laboratory we have found an advantage in choosing stimuli that evoke a response of the simplest type possible. This means reducing features of the stimulus to the minimum number of variables. Once these responses are understood it would make sense to use more sophisticated stimuli. For example, the field pattern over the visual cortex is complicated partly because it is the superposition of effects from sources in both hemispheres of the brain (35). It becomes simpler if activity in only one hemisphere at a time is evoked. This can be accomplished by presenting the visual stimulus in only the left half visual field or the right half field. The image thus appears on the opposite half of the retinas, and by the nature of the neural connections cortical activity appears only in the opposite hemisphere. The lower two maps in Fig. 11 illustrate the observed steady state amplitudes for the VEF (34) when one hemisphere at a time responds. The field leaves the head from one of the indicated regions and enters the other. The stimulus was a grating having a spatial frequency of 5 cycles/degree whose contrast was reversed at 13 Hz. The contrast was 33%, average luminance was 52 cd/m^2 , and the full field display was a circular region encompassed by a visual angle of 9° .

The format for the field maps in Fig. 11 is based on a sphere model for the head, with a globe-like coordinate system. The

"north" and "south" poles lie near the ears, and the equator coincides with the midline. The meridian passes over theinion, which is the slight bump at the base of the skull where muscles attach, and angles are measured with respect to this landmark. The inion is portrayed as the center of each sphere in Fig. 11, and grid points are at intervals of 15° (approximately 2.5 cm distances on the adult head). We chose this format because it was used in the recent work of Darcey et al. (36) who obtained detailed maps of evoked potential distributions by half field stimuli. Consequently we have the opportunity to make a direct comparison of the information provided by the two measures. Darcey et al. obtained transient responses with an array of 40 electrodes placed at the grid points over the posterior region of the scalp. The reference potential was the average potential from all electrodes (37). The stimulus was a red checkerboard pattern of 18 min arc checksize (about 1.5 cycles/degree spatial frequency), with 95% contrast, 68 cd/m^2 average luminance, and 30 ms display time presented in Maxwellian view at infinity to one eye. When the checkerboard was not presented, the 10 degree circular full field viewing screen provided a uniform luminance which matched the average luminance of the checkerboard. Thus in both the VEP and VEF the stimulus was a change in pattern, not luminance.

The first component of the transient VEP measured with a 30 Hz bandwidth was reported to have the same latency of $92 \pm 4 \text{ ms}$ for each of three subjects. The locations of potential extrema and the equipotential patterns remained approximately the same for a period of 20 to 30 ms during which the amplitude rises, reaches its maximum and then decays. The maps for one subject are reproduced in the upper half of Fig. 11 (36). The latency of the VEP is comparable to the latency of the steady state VEF shown in the lower half. Although these responses are for different subjects, there may be some value in comparing them.

For both VEP and VEF the strongest effects are seen over the hemisphere that is contralateral to the half of the visual field presenting the stimulus. The polarity of the magnetic field and of the scalp potential suggest a current dipole source. However the VEP is considerably more widespread than the VEF, in agreement with earlier reports (28). Positive extrema in the potentials are found $\sim 45^\circ$ or more from the midline whereas the field extrema are only $\sim 10^\circ$. Thus volume currents flow through the greater portion of the brain and scalp, but the magnetic field remains fairly well localized near the visual cortex suggesting that they are due to the high-density currents in the immediate vicinity of the active neurons.

Nevertheless Darcey et al. (36) have shown that an assumed dipole source for the potential can accurately predict the pattern. Using a multiple spherical shell model for the head they calculated the position and orientation of the dipole that would give a pattern of equipotentials that best agree with their observations. The predicted depth depends in general on the relative shell radii that are assumed, which can vary substantially among individuals. For illustrative purposes, Darcey et al. chose nominal values, whereby the inner and outer radii of the skull are 90% and 98% of the radius of the scalp. Table 1 summarizes the coordinates for this source as read from the figures in their paper. For comparison we have deduced the location of an equivalent current dipole which would account for the positions of the extrema in the magnetic field. To obtain the depth we first assumed a half space model, and taking the measured distance $\bar{\Delta}$ between extrema deduced the value of " \bar{d} " from Eq. 4. Then we obtained the actual depth " d " by using the correction factor in Fig. 7 appropriate for the 2.4 cm diameter of the pickup coil. This was at most a 15% decrease between " \bar{d} " and " d ". Finally 0.8 cm was subtracted from the value of " d " to account for the distance between the pickup coil and scalp.

The remaining depth for the source below the scalp is tabulated in Table 1. Vertical and lateral positions were determined directly by the position of the midpoint between the field extrema, projected toward the center of the head by a distance equal to the depth of the dipole.

As a second estimate for the source location we took the sphere model with a radius of 10.8 cm to the position of the pickup coil. From the measured angle δ between field extrema we deduced the depth of the current dipole by using the curve in Fig. 8. From this value of "d" we subtracted 0.8 cm to obtain the radial depth below the scalp. The corresponding positions listed in Table 1 for the sources in the two hemispheres do not differ substantially from those deduced by assuming the half space model. Therefore the analysis of the magnetic data to this degree of precision is not sensitive to the assumed shape of the head.

The positions indicated in Table 1 show fair agreement between the VEP and VEF for lateral source coordinates that primarily depend on symmetry features of the maps shown in Fig. 11. Vertical and horizontal positions of the sources lie close to the midline and several centimeters above theinion. The VEF indicates that the left and right hemisphere sources lie somewhat closer together than the sources deduced from the VEP, and in that sense correspond more closely to polarization currents within the cortex at either side of the longitudinal fissure. One outstanding difference between the deduced positions is in the predicted depths of the sources. The VEP predicts a depth below the scalp of 5 cm, whereas the VEF predicts 2 cm. These correspond approximately to 4 cm and 1 cm depths below the surface of the brain when the thickness of the scalp and skull are subtracted. It is informative to compare these predictions with anatomical features of the cortex and its dimensions. A portion of the cortex may be exposed at the occipital pole as illustrated in Fig. 10, but most of its area is found at inner surfaces

Table 1

Location of the current dipole in each hemisphere that best accounts for the observed VEP and VEF mapped in Fig. 11. Vertical and lateral coordinates lie in the plane perpendicular to the radius vector from the center of the head to theinion.

	<u>Stimulus</u>	<u>Vertical Position</u>	<u>Lateral Position</u>	<u>Radial Depth Below Scalp</u>
VEP (reference 36)				
O: JPA	RHF	+ 2.0	- 2.5	+5.5±1 cm
	LHF	2.3	+ 2.0	5.0±0.3
VEF half space model	RHF	3.3	- 1.7	1.6
O: RL	LHF	2.0	+ 0.7	3.2
sphere model	RHF	3.4	- 1.7	1.3
	LHF	2.2	+ 0.7	2.5

of each hemisphere within the longitudinal fissure, with extensions into each hemisphere along the surface of the calcarine fissures which meet the longitudinal fissure at nearly right angles. Anatomical studies of 52 hemispheres collected at autopsy show that the cortex extends inward from the occipital pole to a depth of typically 5 cm (38). Based on studies of the visual effects of war wounds in the cortex, the first centimeter of depth appears devoted to projections of information from the central $\sim 10^\circ$ of the visual field, with more peripheral regions being represented at successively greater depths. Consequently, the depth of the current dipole source deduced from the VEF appears in good agreement with this functional arrangement, since the stimulus included only the central 9° of the visual field. By contrast, the VEP locates the source at a much greater depth, even though peripheral regions of the visual field also were not stimulated.

The reason for this difference is yet to be understood. It is

possible that activity in the cortex is evoked at a much greater depth than previously believed, and the rapid decrease in magnetic field strength with distance from the source favors the closer lying regions in the VEF. If this is true then the VEP and VEF characterize activity in differing regions of the cortex, with the VEP emphasizing the peripheral field. However, this cannot be the case since it is known that foveal stimulation is the major contributor to the VEP. On the other hand, if only the most posterior regions of the visual cortex are active, the volume currents associated with this source evidently become much more widespread at the scalp than is predicted by concentric spherical shell models for the head. The equipotentials appear to be considerably broadened compared with the isochamps than is predicted by lead field calculations for a current dipole (24). A pattern that is anomalously expanded when interpreted with a concentric spherical shell model would imply a source position that is anomalously deep.

It is evident from the VEF shown in Fig. 11 that the current dipole assumed to represent the source in each hemisphere may be tipped at different angles with respect to the midline. Most often they are found to be nearly horizontal, but it is not unexpected to find intersubject differences owing to different placement of the cortex and calcarine fissures in the two hemispheres. Tipping of the source dipoles was also revealed by the analysis of the VEP reported by Darcey et al. (36,37). The angle may vary considerably from one subject to another and between the two hemispheres in the same subject. The potential studies also reveal a feature that has not yet been extracted from the magnetic data: in some cases the dipole is also tipped slightly forwards or backwards. This indicates the presence of a small radial component of the dipole that for the half space or sphere models would not produce an external magnetic field.

Somatically Evoked Response

The somatosensory cortex which responds to stimuli applied to the body is found at quite a different region of the brain than the visual cortex (see Fig. 10). Studies of somatically evoked neural activity can exploit the advantage that responses to stimulation of various regions of the skin project to different areas of the cortex. The map of the projection areas was determined by electrical measurements during neurosurgical operations when portions of the skull above the cortex are removed (39). The first observation of the somatically evoked magnetic field (SEF) by Brenner et al. (40) demonstrated rather sharp localizability of the underlying source, which was found to be near the expected area of the cortex. A repetitive electrical stimulus applied to the little finger produced a steady state evoked field whose center of symmetry could be determined with a precision of better than 1 cm. It was found over the expected position of the Rolandic fissure in the hemisphere contralateral to the side being stimulated. A current dipole source at this position would be perpendicular to the fissure to account for the field pattern. When instead the thumb was stimulated, the pattern shifted along the fissure toward the ear by 2 cm, in correspondence with the positions of the respective projection areas of the cortex (39). The latency of the neuromagnetic response was typically 70 ms for five subjects. No equivalently sharp localizability has been obtained from somatically evoked scalp potentials (SEP). In fact, studies of the transient SEP by Goff et al. (41) show that except for the earliest components 20-30 ms following stimulation potential variations are found on both sides of the head. Recently in our laboratory it has become possible to observe the transient SEF, and direct comparisons of the components of the SEF and SEP have been made (42). The details of some of these studies are reported by Okada et al. (43).

We can apply the analysis developed earlier in this paper

to deduce the position of the current dipole that could give rise to the observed field. For the pattern reported in reference 40 for a stimulus to the little finger the field extrema are separated by $\bar{\Delta} = 4$ cm. Since the pickup coil has a diameter of $2a = 2.4$ cm, Eq. 4 predicts an empirical value of $\bar{d} = 2.8$ cm for the depth of the dipole. Assuming the half space model for the head permits us to use the correction factor in Fig. 7 for the finite size of the pickup coil and deduce an actual depth of $d = 2.4$ cm. Subtracting from this the distance 0.8 cm between the pickup coil and scalp leaves 1.6 cm for the depth of the dipole below the scalp. For a thickness of ~ 1 cm for the scalp and skull we conclude that the source lies within 1 cm of the inner surface of the skull. This value is entirely reasonable if the source represents depolarization currents transverse to the cortex in the primary projection area, where it forms the posterior bank of the Rolandic fissure. For such a near-lying source we can expect that the half space model for the head may be a reasonable approximation when analyzing magnetic effects.

Auditory Evoked Fields

Magnetic fields evoked by auditory stimuli may provide another example of good localizability of cortical activity. A transient evoked field following a click stimulus was discovered by Reite et al. (44) in the region of the Sylvian fissure. Components with latencies in the range of 43-48 ms and 98-118 of opposite field polarity were observed within a localized region of a few centimeters extent; but a corresponding second region of intense field was not reported in their publication, leaving in doubt the exact location of the current source.

Farrell et al. (45) were able to obtain substantially lower background noise in their remote laboratory and identified

two regions of intense field with opposite field directions. One was close to the left temple (two thirds of the distance from EEG position F_7 to F_3) and the other above the left ear (1 cm anterior to the point centered between T_3 and C_3) on the left side of the head. They identified a component having a latency of 50 ms with a positive component of the AEF having a similar latency but showing a maximum amplitude near the top of the head. Because the amplitude of this component in the AEF decreases rather slowly as the pickup coil is moved further from the scalp they argued that it rises from a source lying much deeper than the surface cortex of the brain. Farrell et al. suggested that a source model that would be consistent with the polarities of both the AEF and AEP is a pair of current dipoles lying deep within the temporal lobe, symmetrically placed on both sides of the longitudinal fissure and directed upward.

By contrast with this localization, the auditory evoked potential (AEP) is widespread over the scalp, and no components appear to be localized specifically over the auditory cortex (41). One topic of discussion in the evoked potential literature concerns the problem of finding an "indifferent" location for the reference electrode so as to obtain voltages that are independent of the reference location. Changes in the reference potential may bias the interpretation of potential measurements taken from only a few positions, as has been discussed with regard to the AEP in references 46-48. This problem of seeking an indifferent location is completely avoided in magnetic studies. Nor does the problem seem to introduce uncertainty for the interpretation of evoked potentials obtained by a large array of electrodes, where only the potential differences across the scalp are the basis for subsequent analysis.

More recent magnetic studies by Brenner et al. (35) of the steady state AEP to click stimuli presented at 36 Hz have

provided quantitative data from which the actual depth of the source can be estimated. As remarked by Reite et al. (44) and Farrell et al. (45) the response amplitude is considerably weaker than for the VEF and SEF, which may be due in part to the greater distance of the source from the pickup coil. Only fields near the two extrema could be resolved. The center of the pattern lies over the Sylvian fissure in agreement with the studies cited above. If attributed to a current dipole, the dipole would be directed perpendicular to the fissure. The latency of responses measured for stimulus rates between 27 and 45 Hz was 46 ± 1 ms for one subject, and comparable values were obtained for two other subjects. The field directions on the two sides of the head are the reverse of each other as is consistent with symmetric current flow in the two hemispheres.

Taking the observed separation of $\Delta = 7$ cm between extrema, we deduce from the half space model that the depth below the scalp of the current dipole in each hemisphere is 4 cm. By comparison the sphere model predicts a depth of 3.2 cm. The difference is negligible considering the present accuracy of the data. The predicted depth is sufficiently shallow to represent activity in the portion of the auditory cortex lying within Heschl's gyri, in agreement with reference 45. This extension of the Sylvian fissure is essentially transverse and could thus support depolarization currents in the direction which the current dipole represents. Vaughan and Ritter (46) had suggested that this is the source for a late (200 ms) component of the AEP whose polarity was observed to reverse across the Sylvian fissure, when the nose is the reference position for measuring potentials.

Recently Aittoniemi et al. (49) and Hari et al. (50) reported measurements of quite a different type that provide evidence for evoked activity in the auditory cortex. Magnetic responses were observed during the presentation of a sustained auditory stimulus consisting of a tone at 1 kHz maintained

for 800 ms. They found components of the AEF with latencies of 100 and 180 ms following the onset of the tone that agreed closely in time with components of the AEP. In addition a sustained field extending for the duration of the tone was seen in both records. Amplitude extrema with opposing field directions were found near the estimated ends of the Sylvian fissure and a tangential component of the field connecting them was observed. The variation of the field amplitude with position over the scalp was more pronounced than in the electrical response. From the field pattern and the observed rate at which the field amplitude decreases as the pickup coil is moved away from the scalp Hari et al. concluded that the source lies in the auditory cortex, and not in frontocentral cortical areas as suggested by the location of the strongest AEP (51). Here once again the pattern of evoked field permits a localization of the neural source that the scalp-recorded potentials had not resolved.

Summary

The observed patterns of magnetic field evoked by visual, somatic, and auditory stimuli can be analyzed in first approximation as though arising from current dipole sources. The location of the dipole in each case so far considered is found to lie within the primary projection area of cortical activity for the respective stimulus modality. It is relatively shallow in the case of somatic and visual stimuli, and is considerably deeper for auditory stimuli. The predicted depths are insensitive as to whether the head is approximated as a conducting half space of infinite extent or as a conducting sphere. This is because the observed field patterns are rather sharply localized near their current sources. By contrast the observed evoked potentials reported in the literature are considerably more widespread.

Temporal features of the evoked fields appear physiologically significant. The latencies for steady state responses are

typically 80 ms for patterned visual stimuli of low frequency, 70 ms for somatic stimuli produced by a short current pulse, and 46 ms for auditory click stimuli. Reaction times for visual stimuli of various spatial frequencies vary in the same way as the neuromagnetic latencies as the spatial frequency of the pattern is increased. The difference of 115 ms between the two measures has been attributed to the motor response time, which in a serial model is added to the sensory response time to make up the total reaction time (31). Reaction times to a somatic stimulus when reduced by the value of the latency predict a motor response time of 105 ms (40). Reaction times to a click auditory stimulus obtained by Brenner in our laboratory when reduced by the neuromagnetic latency yield a motor response time of 110 ms. Thus the deduced motor response times are virtually identical across stimulus modalities. This feature lends support to the serial processing model and indicates that steady state magnetic responses designate a physiologically significant time in the sequence of the brain's response to a sensory stimulus.

This brief account shows that during the past 5 years since the discovery of the sensory evoked magnetic field, sufficient progress has been made to demonstrate some of the unique advantages of neuromagnetic techniques for studies of the brain. New and significant results are being obtained at an ever increasing rate. This approach to investigating cortical activity is an important complement of the psychophysical measures of human perception and single cell recordings in animals. It should play an important role in resolving many of the ambiguities that presently exist for interpretations of evoked scalp potentials as well.

We wish to acknowledge our informative discussions with many colleagues; particularly D. Brenner, T. Darcy, E. Maclin and Y. Okada. We are also grateful to T. Darcy, J. Ary, and D.H. Fender for permission to cite their evoked potential data

before publication.

References

- * Supported by the Office of Naval Research Contract N00014-76-C-0568 and by the National Institutes of Health Grants 1 RO1 EY02059-02 and 1 RO1 AM26654-01.
- † Fulbright Senior Research Scholar at the Service de Physique des Solides, Université de Paris XI, 1979-1980.
- 1. Williamson, S.J., Kaufman, L.: Crit. Rev. in Bioengineering, in preparation.
- 2. Williamson, S.J., Kaufman, L.: J. Magn. Magn. Mat., submitted.
- 3. Williamson, S.J., Kaufman, L., Brenner, D.: in Superconductor Applications: SQUIDS and Machines, Schwartz, B.B., Foner, S., Eds., Plenum Publishing, New York, 1977, p. 355.
- 4. Reite, M., Zimmerman, J.E.: Ann. Rev. Biophys. Bioeng. 7, 167 (1978).
- 5. Woodworth, R.S.: Experimental Psychology, Henry Holt and Co., New York, 1938.
- 6. Kaufman, L.: Perception: The World Transformed, Oxford University Press, New York, 1979.
- 7. Jeffreys, D.: in Visually Evoked Potentials in Man: New Developments, Desmedt, Ed., Oxford University Press, New York, 1978.
- 8. Cohen, D.: Science 161, 784 (1968).
- 9. Cohen, D.: Science 175, 664 (1972).
- 10. Reite, M., Zimmerman, J.E., Edrich, J., Zimmerman, J.: Electroenceph. Clin. Neurophysiol. 40, 59 (1976).
- 11. Hughes, J.R., Hendrix, D.E., Cohen, J., Duffy, F.H., Mayman, C.I., Scholl, M.L., Cuffin, B.N.: Electroenceph. Clin. Neurophysiol. 40, 261 (1976).
- 12. Hughes, J.R., Cohen, J., Mayman, C.I., Scholl, M.L., Hendrix, D.E.: J. Neurol. 217, 79 (1977).
- 13. Bleaney, B.I., Bleaney, B.: Electricity and Magnetism, 3rd Edition, Oxford University Press, Oxford, 1976.
- 14. Cohen, D., Hosaka, H.: J. Electrocardiology 9, 409 (1976).
- 15. Grynszpan, F., Geselowitz, D.B.: Biophys. J. 13, 911 (1973).
- 16. Baule, G.M., McFee, R.: J. Appl. Phys. 36, 2066 (1965).
- 17. Baule, G.M.: in Advances in Cardiology, Vol. 10, Rush, S., Lepeschkin, E., Eds., S. Karger, Basel, 1974, P. 304.

18. Plonsey, R.: IEEE Trans. Biomed. Eng. BME-19, 239 (1972).
19. Malmivuo, J.: Acta Polytechnica Scandinavica, Electrical Engineering Series, No. 39, Helsinki, The Finnish Academy of Technical Services, 1976.
20. Jackson, J.D.: Classical Electrodynamics, John Wiley and Co., New York, 1962, p. 142.
21. Tripp, J.H.: in Cardiovascular Physics, Vol. 1, Ghista, D.N., Van Vollenhoven, E., Yang, W., Eds., Karger, Basel, 1979, P. 29.
22. Cuffin, B.N., Cohen, D.: IEEE Trans. Biomed. Eng. BME-24, 372 (1977).
23. Cuffin, B.N., Cohen, D.: J. Appl. Phys. 48, 3971 (1977).
24. Cuffin, B.N., Cohen, D.: Electroenceph. Clin. Neurophysiol. 47, 132 (1979).
25. Regan, D.: Evoked Potentials in Psychology, Sensory Physiology, and Clinical Medicine, Chapman and Hall, London, 1971.
26. Goff, W.R., Allison, T., Vaughan, H.E., Jr.: in Event Related Potentials in Man, Callaway, E., Koslow, S.H., Eds., Academic Press, New York, 1980, in press.
27. Cohen, D.: IEEE Trans. Magn., MAG-11, 694 (1975).
28. Brenner, D., Williamson, S.J., Kaufman, L.: Science 190, 480 (1975).
29. Teyler, T.J., Cuffin, B.N., Cohen, D.: Life Sciences 17, 683 (1975).
30. Zimmerman, J., Edrich, J., Zimmerman, J.E., Reite, M.: in Proc. San Diego Biomedical Symposium, Vol. 17, Martin, J.I., Calvert, E.A., Eds., Academic Press, New York, 1978, p. 217.
31. Williamson, S.J., Kaufman, L., Brenner, D.: Vision Res. 18, 107 (1978).
32. Breitmeyer, B.G.: Vision Res. 15, 1411 (1975).
33. Williamson, S.J., Kaufman, L., Brenner, D.: J. Appl. Phys. 50, 2418 (1979).
34. Brenner, D., Okada, Y., Maclin, E., Williamson, S.J., Kaufman, L.: this volume.
35. Brenner, D., Williamson, S.J., Kaufman, L.: submitted for publication.
36. Darcey, T., Ary, J.P., Fender, D.H.: submitted for publication.
37. Darcey, T.: Ph.D. Thesis, California Institute of Technology, 1979, unpublished.

- 50
38. Stensaas, S.S., Eddington, D.K., Dobbelle, W.H.: *J. Neurosurg.* 4, 747 (1974).
 39. Pennfield, W., Rasmussen, T.: *The Cerebral Cortex of Man*, Macmillan, New York, 1950.
 40. Brenner, D., Lipton, J., Kaufman, L., Williamson, S.J.: *Science* 199, 81 (1978).
 41. Goff, G.D., Matsumiya, Y., Allison, T., Goff, W.R.: *Electroenceph. Clin. Neurophysiol.* 42, 57 (1977).
 42. Kaufman, L., Okada, Y., Brenner, D., Williamson, S.J.: submitted for publication.
 43. Okada, Y.C., Kaufman, L., Brenner, D., Williamson, S.J.: this volume.
 44. Reite, M., Edrich, J., Zimmerman, J.T., Zimmerman, J.E.: *Electroenceph. Clin. Neurophysiol.* 45, 114 (1978).
 45. Farrell, D.E., Tripp, J.H., Norgren, R., Teyler, T.J.: *Electroenceph. Clin. Neurophysiol.*, in press; and this volume.
 46. Vaughan, H.G., Jr., Ritter, W.: *Electroenceph. Clin. Neurophysiol.* 28, 360 (1970).
 47. Picton, T.W., Hillyard, S.A., Krausz, H.I., Galambos, R.: *Electroenceph. Clin. Neurophysiol.* 36, 179 (1974).
 48. Peronnet, F., Michel, F., Echallier, J.F., Girod, J.: *Electroenceph. Clin. Neurophysiol.* 37, 225 (1974).
 49. Aittoniemi, K., Hari, R., Kuusela, M.-L., Katila, T., Varpula, T.: in *Proc. of the Third National Meeting in Biophysics and Medical Engineering in Finland*, Lappeenranta, 1979, Ch. A7.
 50. Hari, R., Aittoniemi, K., Järvinen, M.-L., Katila, T., Varpula, T.: *Technical Report TKK-F-A399*, Department of Technical Physics, Helsinki University of Technology, 1979; and this volume.
 51. Picton, T., Woods, D., Stuss, D., Campbell, K.: in *Multi-disciplinary Perspectives in Event-Related Brain Potential Research*, Otto, D., Ed., U.S. Government, Washington, D.C., 1978, p. 515.

D
FI
8
—